MATERIALS FOR ROBOTICS

# Self-powered locomotion of a hydrogel water strider

**Hong Zhu[1], Borui Xu[1], Yang Wang[1], Xiaoxia Pan[2], Zehua Qu[2], Yongfeng Mei[1]***



**Hydrogels are an exciting class of materials for new and emerging robotics. For example, actuators based on hydrogels have impressive deformability and responsiveness. Studies into hydrogels with autonomous locomotive abilities, however, are limited. Existing hydrogels achieve locomotion through the application of cyclical stimuli or chemical modifications. Here, we report the fabrication of active hydrogels with an intrinsic ability to move on the surface of water without operated stimuli for up to 3.5 hours. The active hydrogels were composed of hydrophobic and hydrophilic groups and underwent a dynamic wetting process to achieve spatial and temporal control of surface tension asymmetry. Using surface tension, the homogeneous active hydrogels propelled themselves and showed controlled locomotion on water, similar to common water striders.**

## INTRODUCTION

Basilisk lizards (*1*), water snails (*2*), *Mesovelia* (*3*), and water striders (*4*, *5*) can move freely on the surface of water. With an average velocity of 60 body lengths per second, water striders use their central hydrophobic legs to strike the water surface in a sculling motion. During the strike, fore-aft contact force differences between the central hydrophobic legs are generated as a propulsive force and overcome resistances to move freely (*6*). To mimic the locomotion of water striders and move freely on water surfaces, self-propelled devices have been developed and driven by various external fields (*7*–*10*). As major components of tissues in living species, hydrogels are polymer networks that are infiltrated with water and have excellent properties of high water content, softness, and stimuli responsiveness. Under external stimuli (e.g., optical, electrical, hydraulic, or magnetic changes), hydrogels can convert other forms of energy to generate deformations and forces, which are induced by the osmotic pressure change of hydrogels responding to external stimuli (*11*, *12*). These existing strategies to achieve autonomous locomotion in hydrogel materials involve applying cyclical stimuli (*13*–*17*), which requires peripheral devices and an energy source. In this study, we endowed hydrogels with the ability to locomote on the water surface by continuously establishing asymmetric surface tensions through the dynamic wetting process of active hydrogels.

## RESULTS

### Locomotion of hydrogel water striders and mechanisms of locomotion

We collected common water striders from local freshwater ponds to observe and understand their locomotion. The middle legs of water striders moved backward to generate fore-aft asymmetric contact angles from the strider legs (Fig. 1A and inset). The curvature force caused by the asymmetric contact angles (unequal α and β) worked as dominant propulsive force for the water surface locomotion of water striders. After the driving strike, the water striders dragged the middle legs forward for recovery and then went on for the next thrust. During the recovery, only resistive force existed. Thus, the velocity of the water strider increased sharply from 21.21 to 37.50 cm/s in the thrust stage of 0.008 s and decreased slowly to 21.21 cm/s in the recovery stage of 0.013 s. In the next 0.008 s, the velocity of the water strider increased rapidly to 37.62 cm/s, again owing to the strike of middle legs. Then, the velocity of water strider decreased slowly to 19.21 cm/s in the following 0.017 s. In the whole 0.05 s, the water strider glided forward 5.24 cm (Fig. 1B). Inspired by common water striders, we synthesized an active hydrogel poly(hydroxyethyl methacrylate-co-acrylic acid) [p(HEMA-co-AA)] that could move autonomously on the water surface for 210 min without external energy input. The superimposed time-lapse snapshots and corresponding color-indicated trajectory of this hydrogel water strider's locomotion in the first 4 s are shown in Fig. 1C. We proposed that the propulsion mechanism of this autonomous locomotion is based on the dynamic wetting process of the active hydrogel (Fig. 1C, inset). The active hydrogel consisted of long carbon chains, hydroxyl groups, and ester groups (fig. S1). The methyl groups on the backbone of the hydrogel network were hydrophobic, and the hydroxyl groups on the side chains were hydrophilic. When the pristine hydrogel was placed in air, it preferentially exposed the nonpolar parts of the backbone toward the air to minimize surface energy. Thus, the pristine hydrogel water strider was unwetted. During the water intake and swelling process, the hydroxyl groups migrated to the surface to minimize the interfacial free energy (*18*–*23*). The reorientation of the hydrophobic and hydrophilic groups occurred at the outermost interface between 5 and 10 Å (*19*). Then, the hydrogel became wetted, and the water intake increased the total mass of the hydrogel, which slightly sank relative to the air-water interface and exposed the new unwetted part to water. We defined this process as the dynamic wetting process of the active hydrogel. The dynamic wetting process occurred unevenly at the water-air interface surrounding hydrogel, which caused an uneven and varying distribution and a good spatial and temporal control of surface tension around the hydrogel. According to the Marangoni effect, the local inhomogeneous distribution of surface tension causes a convection flow of liquid, and then, floating objects move toward the higher surface tension regions (*24*). Therefore, the hydrogel moved toward the nonwetting region with a fluctuating velocity. The velocity fluctuated throughout the locomotion owing to the dynamic wetting process, and the initial velocity of the locomotion is 4.86 cm/s. After 15 min, the velocity increased sharply from 1.33 to 2.32 cm/s in 0.167 min and decreased slowly down to 1.51 cm/s in the subsequent 0.666 min, which showed a similar fluctuation to the velocity

[1]Department of Materials Science, State Key Laboratory of ASIC and Systems, Fudan University, 200433 Shanghai, P. R. China. [2]Department of Macromolecular Science, State Key Laboratory of Molecular Engineering of Polymers, Fudan University, 200433 Shanghai, P. R. China.
*Corresponding author. Email: yfm@fudan.edu.cn

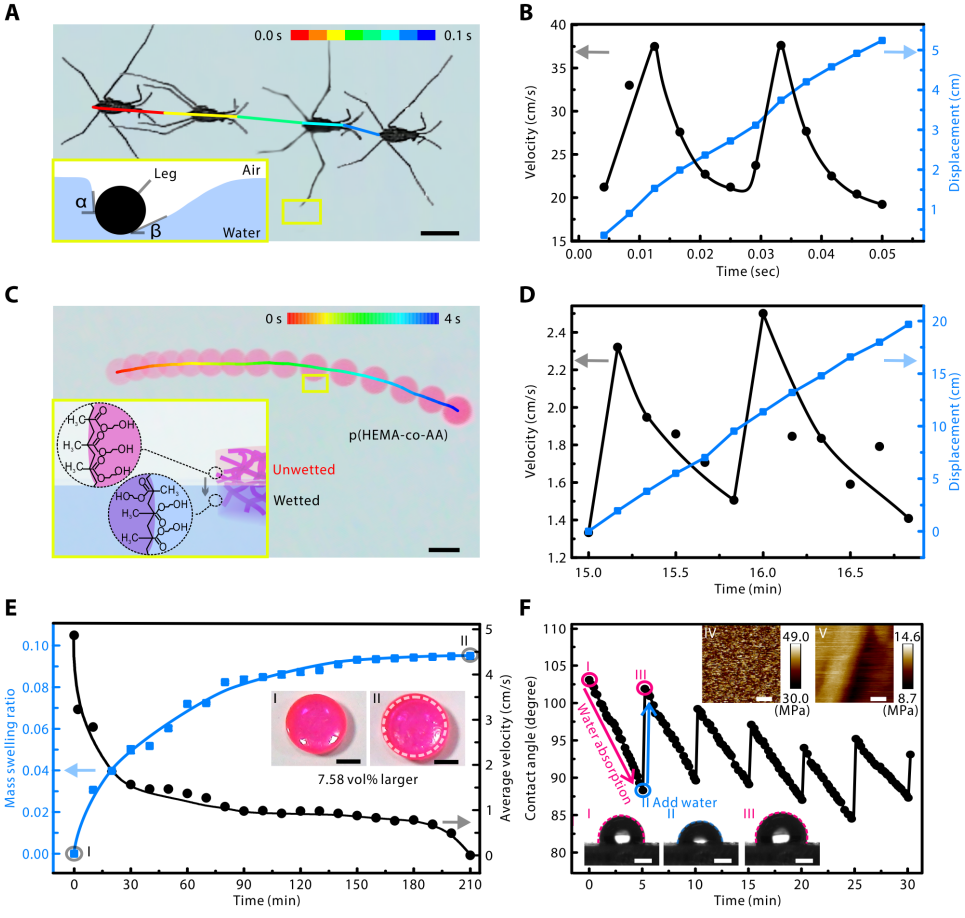


**Fig. 1. Motion and mechanism of common water strider and hydrogel water strider.** (**A**) Superimposed time-lapse snapshots and corresponding color-indicated trajectory of common water strider in 0.1 s. The inset is a schematic illustration of propulsion mechanism of common water strider. Here, α and β are contact angles of the strider leg. (**B**) The velocity and displacement of the common water strider. (**C**) Superimposed time-lapse snapshots and corresponding color-indicated trajectory of hydrogel water strider in 4 s. The inset is a schematic illustration of the propulsion mechanism of hydrogel water strider. (**D**) The velocity and displacement of the hydrogel water strider. (**E**) Mass swelling ratio and average velocity changes during the whole locomotion time. The insets are photos of the hydrogel at 0 min (I) and 210 min (II). The dashed line is the initial edge of the hydrogel. (**F**) Contact angle changes of hydrogel in the first 30 min. The bottom insets are the photographs of contact angle at states I, II, and III. The top insets are the in situ AFM microscopic modulus of hydrogel after adding water for 0 min (IV) and 80 min (V). Scale bars, 5 mm (A), 1 cm (C), 2 mm [insets of (E)], 1 mm [bottom inset of (F)], and 100 nm [top inset of (F)].

of the water strider locomotion. The hydrogel water strider moved 19.69 cm in 1.83 min (Fig. 1D). The surface tension–dominated locomotion of the hydrogel water strider matched the agility of the common water strider, with fluctuating speed and long-lasting locomotion duration.

To verify the propulsion mechanism of the hydrogel water strider's locomotion, we analyzed the velocity of locomotion and conducted characterization to the hydrogel. The velocity was tracked from the recorded video, and we calculated the average velocity per 5 min (Fig. 1E, black line). The initial velocity was 4.86 cm/s, and it dropped to 1.565 cm/s in the first 30 min. Then, the velocity was steady around 1 cm/s during the following 150 min and lastly decreased markedly to 0 cm/s in the last 30 min. Then, we analyzed the instantaneous velocity and frequency of velocity changes through the fast Fourier transform (fig. S2). The frequency of velocity changes gradually decreased from 0.1504 to 0.0231 Hz in the first 40 min. The blue line in Fig. 1E indicates the mass swelling ratio of the hydrogel changing with time, where the mass swelling ratio is the weight difference between the swollen hydrogel and initial hydrogel over the weight of the initial hydrogel. The mass swelling ratio increased markedly from 0 to 0.049 in the first 30 min and then increased slowly to 0.094 in the following 150 min. In the last 30 min, the mass swelling ratio of the hydrogel gradually reached to the equilibrium of 0.095. The slope of mass swelling ratio increase was consistent with the slope of velocity decrease, which suggested that the water intake of hydrogel is related to the velocity of locomotion. Therefore, adding a water-sensitive dye into the hydrogel as an indicator, the velocity of the hydrogel water striders could be visualized via the water content and color changing of the hydrogel (fig. S3). Moreover, the insets of Fig. 1E visually show the volume changes of the hydrogel. The volume of the hydrogel was 7.58% larger than that of the pristine one after the whole swelling process. Considering the relationship between the velocity and water intake process, we conducted characterizations of the hydrogel at the microscopic level during the water intake process. To verify that the dynamic wetting occurs during the water intake process, we measured the contact angles of the hydrogel by the sessile droplet technique (Fig. 1F). The initial contact angle was 103.1° (state I), which means that the pristine hydrogel surface was hydrophobic. In the first 5 min, the hydrogel absorbed water from the droplet, and the contact angles gradually decreased to 88.3° (state II). Afterward, when another droplet of the same volume was added on the same place of hydrogel, the contact angle increased to 101.9° (state III) immediately, which means that the adjacent part of the first droplet on the hydrogel was still hydrophobic. The bottom inset photos of Fig. 1F directly compare the droplet volume and contact angle at states I, II, and III. The droplet volume decreased from state I to II owing to water absorption and became larger at state III than state II because of droplet addition. The pristine hydrogel was unwetted, and then, the part of the hydrogel that had contact with the water droplet changed to a wetted condition because of water absorption. However, the adjacent part was still unwetted. With more added water, the adjacent part of the hydrogel started changing to a wetted condition. This wetting process of the hydrogel continued for a long time, but for simplicity, we just examined the first 30-min results of contact angle changes. After 210 min of locomotion, the surface of the active hydrogel was wetted, and the contact angle was 65.1°, which decreased to 48.1° with the

addition of the new droplet. Before the hydrogel was wetted, water diffused into the interior of the hydrogel instead of spreading along the surface. Moreover, from the rheological test, in situ fast-scan atomic force microscopy (AFM), and cryo–scanning electron microscopy (SEM) results, we observed that the elastic modulus of the hydrogel dropped markedly, and the morphology of the hydrogel changed from flat to rough during the water intake and dynamic wetting process (fig. S4). The microscopic elastic modulus of the hydrogel at the original state had a value ranging from 30.0 to 49.0 MPa (state IV); then, it dropped to a range of 8.7 to 14.6 MPa after the 30-min water intake (state V). After 80 min, the hydrogel became soft and the elastic modulus markedly decreased to a range from 7.4 to 8.1 kPa. Combining the synergistic variation slope of velocity and mass swelling ratio as well as the microscopic changes during the water intake and dynamic wetting process, we posit that the propulsion mechanism of the locomotion was based on a dynamic wetting process and the Marangoni effect. The hydrogel absorbed water, which caused the hydrophobic groups at the outermost surface of hydrogel to turn inside and the hydrophilic groups to reorient toward the outside. The hydrogel was dynamically wetted during the reorientation of the functional groups, which was macroscopically shown as a change in contact angle. The continuous reorientation processes of the active hydrogel induced surface tension changes, and the propulsion force of the locomotion changed relatively, according to the Marangoni effect. Because the mechanism of the locomotion depends on the dynamic wetting process of the hydrogel and Marangoni effect, this autonomous locomotion was reversible as long as the hydrogel was exposed to repeated dehydration (fig. S5).

### Versatility of active hydrogels

Hydrophobic hydrogels with different cross-linker amounts and types all showed autonomous locomotion on water surface (Table 1 and fig. S6). We first analyzed the locomotion and swelling behaviors of the p(HEMA-co-AA) hydrogel with different cross-linker amounts ranging from 0.5 to 10 volume %. The mass swelling ratio of hydrogels after absorbing water for 5 min over the equilibrium mass swelling ratio was defined as the initial water intake percentage. The initial water intake percentage increased from 0.30254 to 0.59741, with the cross-linker amounts increasing from 0.5 to 10 volume %. After swelling equilibrium, the hydrogel with 0.5 volume % cross-linker showed the highest equilibrium mass swelling ratio of 0.09602, and the initial water intake percentage decreased to 0.02931 when the cross-linker was added to 10 volume %. The hydrogel with 0.5 volume % cross-linker took 280 min to reach the swelling equilibrium, and the time gradually decreased to 85 min, with the cross-linker increasing to 10 volume %. The p(HEMA-co-AA) hydrogel with different cross-linker amounts were all able to locomote. The initial velocity of the locomotion increased from 4.78 to 7.07 cm/s, with the cross-linker amounts increasing from 0.5 to 10 volume %, which showed a similar trend to the initial water intake percentage. In addition, the locomotion duration was slightly shorter than the equilibrium swelling time. The hydrogel with 0.5 volume % cross-linker had the ability to move on the water surface for 270 min. With the increasing of cross-linker amounts from 0.5 to 10 volume %, the locomotion duration decreased from 270 to 55 min. The initial water intake percentage revealed the water affinity of hydrogel. With the increase in cross-linker amounts, the pore size decreased and the cross-link ratio of the hydrogel increased relatively. With a smaller pore size, the hydrogel showed a stronger water affinity and higher initial water intake percentage. Because of the increase in the cross-link ratio, the cross-link density increased (*25*). According to the Flory-Rehner theory, including the ideal Donnan equilibria (*26*), the equilibrium mass swelling ratio depends on the charge density, cross-link density, and relaxed volume fraction. With the same functional groups, the high equilibrium mass swelling ratio can be acquired at low cross-link density. Thus, the equilibrium mass swelling ratio increased with increasing cross-linker amounts, as shown above. Considering the relationship between the mass swelling ratio, locomotion velocity, and locomotion duration, the initial velocity was consistent with the initial water intake percentage, and the locomotion duration was consistent with the equilibrium mass swelling ratio and equilibrium swelling time. The AFM images of the p(HEMA-co-AA) hydrogel with different cross-linker amounts ranging from 0.5 to 10 volume % showed the micromorphologies of the active hydrogel with different cross-linking densities (fig. S7). In addition, the contact angles of the p(HEMA-co-AA) hydrogel with different cross-linker amounts changing with time verified the dynamic wetting process of the active hydrogel with different cross-linking degrees (fig. S8). Moreover, not only did the hydrogel p(HEMA-co-AA) show the ability to move on water surface spontaneously, but other types of acrylic derivative hydrogels, such as pHEMA and poly(methacrylic acid) (pMA), also had locomotive ability. We compared and analyzed the swelling and locomotion behaviors of these active hydrogels with the same cross-linker amounts (1 volume %). The initial water intake percentage of p(HEMA-co-AA),

**Table 1. Comparison of swelling behaviors and locomotion of hydrogels with different cross-linker amounts and types.**

| Type | Cross-linker amount | Initial water intake percentage | Equilibrium mass swelling ratio | Static equilibrium swelling time (min) | Locomotion capability | Locomotion duration (min) | Initial velocity (cm/s) |
|---|---|---|---|---|---|---|---|
| p(HEMA-co-AA) | 0.5 volume % | 0.30254 | 0.09602 | 280 | Yes | 270 | 4.78 |
| | 1 volume % | 0.32512 | 0.09498 | 210 | Yes | 210 | 4.86 |
| | 2 volume % | 0.40747 | 0.06798 | 160 | Yes | 150 | 5.31 |
| | 5 volume % | 0.56476 | 0.03042 | 110 | Yes | 100 | 5.66 |
| | 10 volume % | 0.59741 | 0.02931 | 85 | Yes | 55 | 7.07 |
| pHEMA | 1 volume % | 0.29692 | 0.01721 | 60 | Yes | 50 | 4.65 |
| pMA | 1 volume % | 0.27466 | 0.01602 | 40 | Yes | 30 | 4.66 |
| AH | 0.1 M | 0.98333 | 4.22957 | 140 | No | 0 | 0 |

pHEMA, and pMA were 0.32512, 0.29692, and 0.27466, respectively. The equilibrium mass swelling ratio, static equilibrium swelling time, and locomotion duration showed large differences between these three hydrogels. The equilibrium mass swelling ratio of p(HEMA-co-AA) reached 0.09498; however, the ratios of pHEMA and pMA were just 0.01721 and 0.01602. The equilibrium swelling times were 210, 60, 40 min for p(HEMA-co-AA), pHEMA, and pMA, respectively. All these active hydrogels had the ability to locomote as well. The initial velocity of p(HEMA-co-AA) was 4.86 cm/s, which was largest among all the three hydrogels. The initial velocities of pHEMA and pMA were 4.65 and 4.66 cm/s, respectively, and the locomotion durations were 210, 50, and 30 min for p(HEMA-co-AA), pHEMA, and pMA, respectively. Comparing pHEMA with p(HEMA-co-AA), the copolymerized acrylic acid monomer provides ionic groups to the hydrogel, which increases the affinity to water simultaneously. Thus, the initial water intake percentage of p(HEMA-co-AA) was slightly higher than pHEMA. In addition, an increasing number of ionic groups produce additional osmotic pressure that swells the hydrogel (*26*). Thus, the equilibrium mass swelling ratio of p(HEMA-co-AA) was much higher than pHEMA. As for the pHEMA and pMA, the types and amounts of functional groups are almost the same, so the initial water intake percentage and the equilibrium mass swelling ratio are almost the same. Thus, the initial velocity of these three hydrogels was consistent with the initial water intake percentage, and the locomotion duration was consistent with the equilibrium mass swelling ratio and static equilibrium swelling time. However, pristine hydrophilic hydrogel, such as calcium alginate hydrogel (AH), showed no locomotion on a water surface owing to the nonexistence of the dynamic wetting process. Thereafter, we extended the range of liquids with different surface tension coefficients (fig. S9) and different pH values (fig. S10), which the hydrogel could also move automatically on. Using pH-sensitive dye as an indicator, the velocity of the hydrogel on aqueous solutions with different pH values could be visualized as well. All these active hydrogels could be processed by both three-dimensional (3D) printing and soft mold casting (fig. S11). Therefore, hydrogel water striders made of various active hydrogels with different cross-linking degrees could move on diverse aqueous solutions with a suitable surface tension range, which demonstrated the universality of the autonomous locomotion of the active hydrogel.

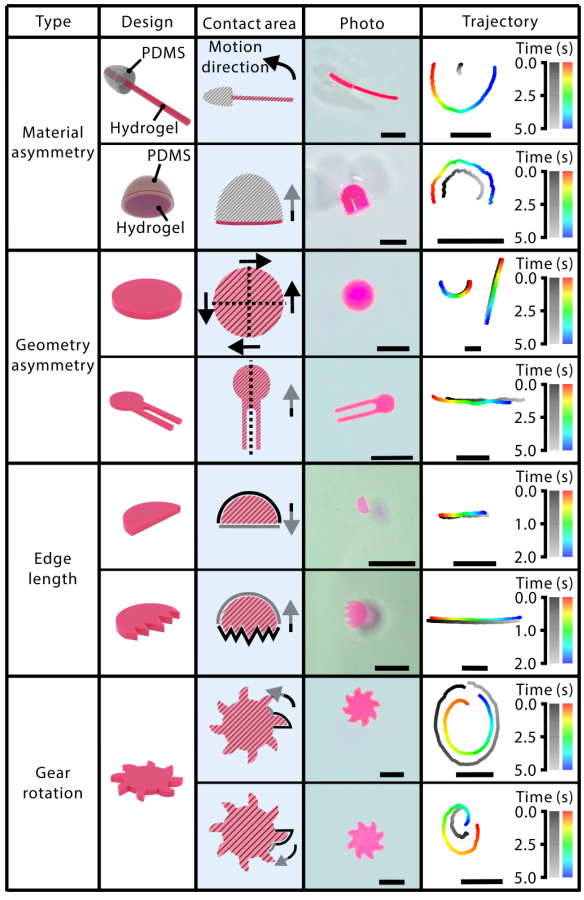


**Fig. 2. Materials and geometry asymmetry of hydrogel water striders and relative locomotion.** Design, contact area, photo, and trajectory of material asymmetric hydrogel water striders (first and second rows); geometry asymmetric hydrogel water striders (third and fourth rows); asymmetric hydrogel water striders with different edge lengths (fifth and sixth rows); and hydrogel water striders in a gear shape (seventh and eighth rows). To distinguish the linear and angular velocity, the trajectories of gradient gray color were tracked from the central positon of the hydrogel water strider and the trajectories of gradient rainbow color were tracked from the edge positon. Scale bars, 1 cm (first to third, seventh, and eighth rows in the fourth column), 2 cm (fourth to sixth rows in the fourth column), 5 cm (first to sixth rows in the fifth column), and 3 cm (seventh and eighth rows in the fifth column).

## Guided locomotion by materials or geometry design

The locomotion of hydrogel water striders was controlled by introducing material asymmetry, geometry asymmetry, and edge length difference to hydrogel water striders through different kinds of processing methods. As illustrated in the first two rows of Fig. 2 (movie S1), material asymmetry was realized by coating the hydrogel with hydrophobic polydimethylsiloxane (PDMS). There was only one side of the hydrogel in contact with water, as shown in the third column of the first two rows in Fig. 2. The photo of the hydrogel water striders and the trajectories of their locomotion are shown in the fourth and fifth column of the first two rows in Fig. 2. The trajectories of gradient gray color were tracked from the central positon of the hydrogel water strider, and the trajectories of gradient rainbow color were tracked from the edge positon to distinguish the linear and angular velocity of the hydrogel water strider. With a longer tail in the first row in Fig. 2, the hydrogel water strider rotated around the mass center. With only one surface of hydrogel exposed to water in the second row in Fig. 2, the hydrogel water strider moved in a circular path. As discussed before, the surface tension at the hydrogel surface dynamically decreased owing to the dynamic wetting process, whereas the surface tension at the PDMS surface remained steady. Thus, the surface tension differences between the hydrogel and PDMS surface pushed the hydrogel water strider to the more hydrophobic surface, which was the PDMS surface. Geometry asymmetry also played a vital role in the locomotion of the hydrogel water strider (movie S2). When the hydrogel water strider was in a central symmetric shape, the contact area was centrally symmetrical. So, the locomotion direction was arbitrary, and the trajectory of the locomotion was either circular or linear. The ratio of circular motion was higher with larger hydrogel diameters (fig. S12). The photos and locomotion of a hydrogel water strider in a round shape are given in the third row of Fig. 2. After two rectangular tails were added to the round shape, the hydrogel water strider moved in a straight line toward the round shape surface (fourth row in Fig. 2). In the simple semicircle shape, the hydrogel water

strider moved linearly toward the straight-line surface (fifth row in Fig. 2). In the semicircle shape with zigzag edge, the hydrogel water strider moved linearly toward the curved-line surface (sixth row in Fig. 2). For hydrogel water striders with asymmetric geometries, one side of the hydrogel had a larger water-hydrogel interfacial area, which had more contact with water and a relatively lower surface tension than the other side. Therefore, the hydrogel water strider moved linearly toward the side with a shorter edge length, which means a smaller water-hydrogel contact area. Adding one quarter circle as a vane and transforming the circle into a gear shape was another way to break the symmetry of the circular hydrogel water strider (seventh and eighth rows in Fig. 2 and movie S3). When the curved teeth edge was at the counterclockwise position of the straight teeth edge, the gear rotated counterclockwise. When the reverse side contacted the water, the gear rotated clockwise. Because surface tension is always perpendicular to the gear boundary in the gear shape, the disequilibrium angular momentum led to the rotation toward the curved teeth edge in each gear vane (*27*). Thus, the hydrogel water strider could realize multiple locomotion types and could be controlled through both material and geometric design.

## Guided locomotion by interactions with surroundings

Despite the material and geometry of the hydrogel water strider itself, the locomotion could also be controlled by surroundings. The hydrogel water strider could demonstrate hydrophobic features as it got close to a boundary. To minimize the interfacial free energy (*28*, *29*), the hydrogel water strider repelled and moved away from the hydrophilic boundary, while it attracted and stuck onto the hydrophobic boundary (fig. S13). When the hydrogel water strider with diameter $D$ moved in a confined environment with hydrophilic boundaries and an opening (opening length equal to $d$), the locomotion of the hydrogel water strider could be controlled through the relationships between $d$ and $D$. When $d$ was equal to 0, the hydrogel water strider moved in the confined environment with wall-following trajectories (first row in Fig. 3 and movie S4). The experimental results showed the trajectories of hydrogel in triangular, square, four-pointed star, and circular containers. Within the triangular container, the hydrogel moved from one vertex to the opposite edge and was then repelled back or moved to another adjacent vertex. Within the square container, the hydrogel followed the shape of the container, and the trajectory looked like a square. Within the four-pointed star container, the hydrogel moved from one vertex to the adjacent vertex and then moved back or to the other adjacent vertex. As for the circular container, the hydrogel moved in circular paths with different radii. The trajectories bear a resemblance to the container shape with several random paths. The intrinsic tendency of active swimmers to move near boundary surfaces guides the hydrogel water striders close to the boundary (*30*, *31*), and owing to boundary limitations, the number of freedom degrees is reduced, which leads the hydrogel water striders to move along the wall (*32*). In addition, the hydrophilic and hydrophobic interactions between the hydrogel water striders and the hydrophilic boundary kept the hydrogel water striders from getting stuck onto the boundary. When $d$ was smaller than $D$, the hydrogel moved periodically around the opening (second row in Fig. 3 and movie S5). The hydrogel whirled three cycles in the circular paths with an opening and lastly stopped around the opening. When $d$ was larger than $D$, the hydrogel moved away from the hydrophilic boundaries and out of the confined environment from the opening

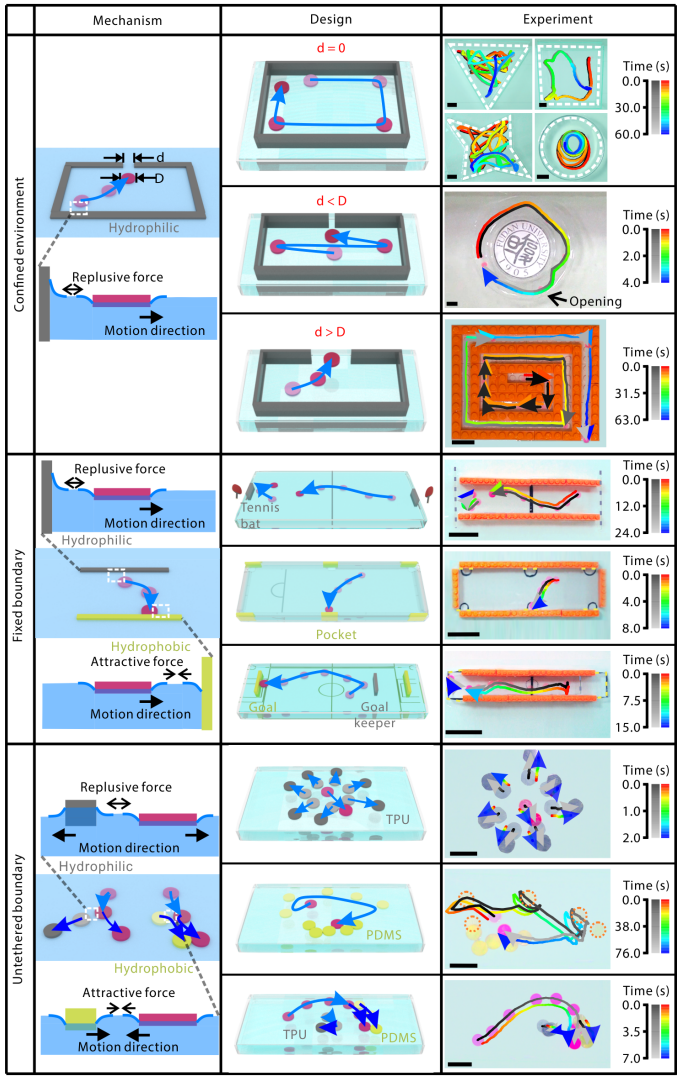


**Fig. 3. Locomotion of hydrogel water striders in different environments.** Mechanism, design, and experiment of hydrogel water striders' locomotion in a confined environment (first to third rows); in an environment with fixed boundaries (fourth to sixth rows); and in an environment with untethered boundary (seventh to ninth rows). Scale bars, 2 cm (first to third and seventh to ninth rows) and 5 cm (fourth to sixth rows).

(third row in Fig. 3 and movie S5). Thus, the hydrogel could find the path and pass through the maze directly without veering onto the wrong path. The confinements from all directions reduced the number of freedom degrees and constrained the locomotion of the hydrogel water striders. The opening in the confined environment allowed a small amount of freedom and relieved the constraints to some extent (*33*). On the basis of the same mechanisms of hydrophilic and hydrophobic interactions, the hydrogel water striders could be controlled to mimic several ball games with a fixed boundary. The table tennis playing surface was composed of hydrophilic glass and acrylonitrile-butadiene-styrene plastic (in orange), which all exerted a repulsive force on the hydrogel water strider. Thus, in the table tennis playing surface, the hydrogel water strider moved toward hydrophilic glass at the left side (as tennis bat) and was repelled back (fourth row in Fig. 3 and movie S6). In contrast, to imitate

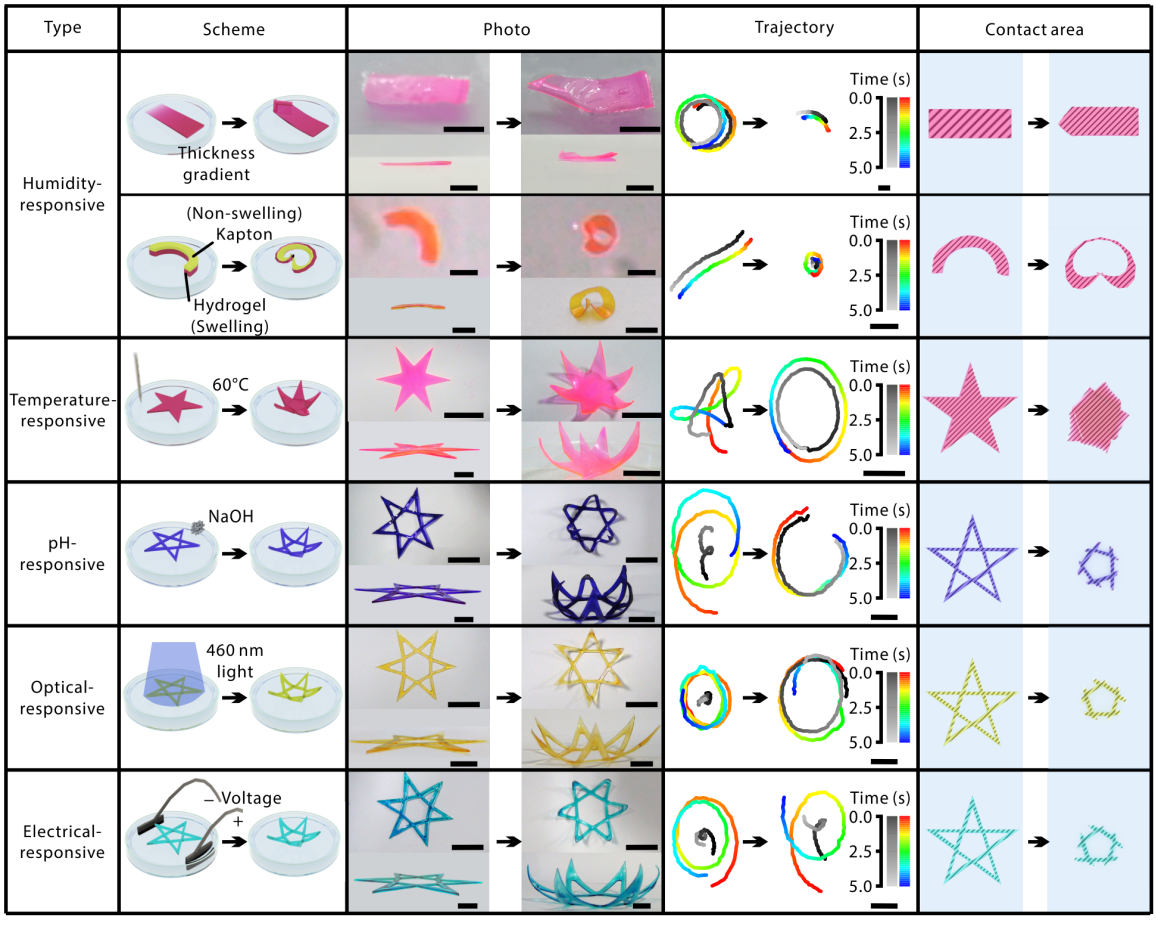


**Fig. 4. Stimuli-responsive hydrogel water striders.** Scheme, photo (top view on the top and side view on the bottom), trajectory, and contact area comparisons of different types of stimuli-responsive hydrogel water striders before and after stimulus was applied. Scale bars, 2 mm (first row in the third column), 5 mm (second row in the third column), 2 cm (top view photos of the third to sixth rows in the third column), 1 cm (side view photos of the third to sixth rows in the third column), and 5 cm (all in the fourth column).

the pocket of billiards, we pasted six hydrophobic polypropene (PP) thin films onto the boundary walls, which exerted an attractive force to the hydrogel water strider. After the hydrogel water strider was put in the playing area, it was attracted and stuck to the PP thin film (fifth row in Fig. 3 and movie S6). Combining these two kinds of interactions in the football field, the hydrophobic PP films worked as the goal, and the hydrophilic glass worked as the goalkeeper. The hydrogel water strider was repelled by the glass and changed the moving direction to the other goal. After moving into the goal area, the hydrogel water strider was attracted to the goal and stuck onto it, which mimicked the short-range shot and score (sixth row in Fig. 3 and movie S6). Applying the understanding of hydrophilic and hydrophobic interactions between the hydrogel and surrounding objects to an untethered boundary, object manipulation could be realized through the hydrogel water strider. When the hydrogel water strider was surrounded by seven floating hydrophilic thermoplastic polyurethane (TPU) membranes, it expelled all TPU membranes at the same time and moved away from them (seventh row in Fig. 3 and movie S7). In contrast, the hydrogel water strider came close to and carried five randomly distributed PDMS pieces together one by one (eighth row in Fig. 3 and movie S7). The mass of one PDMS piece was slightly higher than that of the hydrogel water strider, which showed the potential of transporting cargos and pollution collection. We treated a water surface contaminated by 50 plastic balls via the hydrogel water strider, and 49 of them were collected together (fig. S14 and movie S10). Although the target (yellow PDMS piece) was hindered by a barrier (gray TPU membrane), the hydrogel water strider could bypass the barrier and navigate to the target on the basis of the hydrophilic and hydrophobic interaction mechanism (ninth row in Fig. 3 and movie S7). Applying the understanding of the long-range hydrophilic and hydrophobic interactions between the hydrogel and surroundings, the wettabilty of a given surface could be identified by the hydrogel water strider, which could be applied to oil exploration (fig. S14 and movie S10). On the basis of the simple hydrophilic and hydrophobic interaction mechanisms, the hydrogel water strider could be controlled to migrate in a directional movement toward the aimed targets, which demonstrated the potential to conduct complex missions on a liquid surface.

## Deformable locomotion by stimuli-responsive active hydrogels

Using several types of stimuli-responsive hydrogels, the hydrogel water striders showed different locomotion before and after stimuli were applied. Humidity-responsive hydrogel water striders were realized

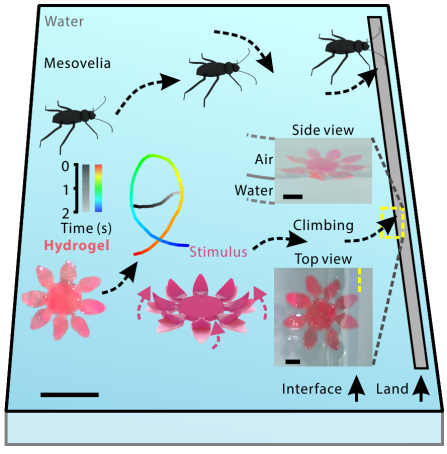


**Fig. 5. All kinds of locomotion of hydrogel water striders and common water striders, including freewill moving on water surface and menisci climbing.** The top part is the locomotion of *Mesovelia* with freewill gliding and ascending menisci onto land. The bottom part is the locomotion of hydrogel water striders. The left one is a photo of the flower-shaped humidity-responsive hydrogel and the trajectory of its locomotion in 2 s. The middle one is the schematic illustration of changes in the hydrogel under humidity stimulus. The right two are the photos of hydrogel water striders climbing the menisci and attached to the target position in the top and side view. Scale bars, 4 and 1 cm (top view and side view of the photos).

by two ways. The first way was to establish a thickness gradient in the rectangular thin film, as the scheme shows (second column in the first row in Fig. 4). After coming into contact with water, the thinner part of the hydrogel thin film deformed more quickly and curved to a smaller radius such that the flat hydrogel thin film changed to an arc shape with two sides curved (third column in the first row in Fig. 4). Correspondingly, the trajectory of the locomotion changed from circular to nearly linear in 5 s (fourth column in the first row in Fig. 4 and movie S8). This was because the contact area of the hydrogel changed from a rectangle to an arrow shape (fifth column in the first row in Fig. 4) (*34*). The second way was to add a non-swelling Kapton on top of the swelling hydrogel, and then, the hydrogel water strider changed its shape from a flat arc to a closed curved band shown in the second and third columns in the second row in Fig. 4. In 5 s, the hydrogel water strider moved in a straight line and then changed to a circular motion after stimulus was applied (fourth column in the second row in Fig. 4 and movie S8). The contact area of the hydrogel water strider changed from an arc shape to a closed heart-like shape, which affected the locomotion (fifth column in the second row in Fig. 4). *N*-isopropyl acrylamide (NIPAM) was introduced into the hydrogel to endow our active hydrogels with responsiveness to temperature. It had a flat pentagram shape and changed to curved five-point pentagram after being heated to 60°C. The trajectory of the temperature-responsive hydrogel water strider changed from a combination of rotation and circular motion to circular motion only (fourth column in the third row in Fig. 4 and movie S8). This depended on the contact area of the temperature-responsive hydrogel water strider changing from a pentagram to an irregular pentagon. By including acrylic acid, adding azobenzene, or adding 2-acrylamido-2-methylpropane sulfonic acid (AMPS) into hydrogels, pH-responsive, light-responsive, or electrical-responsive active hydrogels were synthesized, respectively. Before stimulus was applied, their shape was a flat, hollowed-out pentagram. The hydrogel water striders changed to a curved five-point pentagram after adding NaOH into water, irradiating 460-nm light, or applying voltage to the electrode in the phosphate-buffered saline buffer solution. Their locomotion shifted from rotation with slightly random translation to a circular motion (fourth column in the fourth to sixth row in Fig. 4 and movie S8). These depended on the contact area of the hydrogel water strider transforming from a hollowed-out pentagram to an irregular hollowed-out pentagon. With designed geometry, the hydrogel water strider composed of temperature-responsive and normal active hydrogel showed controlled locomotion through heating the water (fig. S15). By applying stimuli-responsive active hydrogels, the geometry of the hydrogel water striders could be altered under stimulus on demand during the locomotion, which changed the locomotion of the hydrogel water strider correspondingly. With elaborate design, the locomotion of the stimuli-responsive active hydrogel water strider could be controlled under stimuli.

### Biomimetic locomotion by hydrogel water striders

Because they are capable of deforming under certain stimulus as desired, the hydrogel water striders could mimic other locomotion of common water striders. Besides gliding on water surface, common water striders sometimes need to seek land and climb menisci to avoid predators or lay eggs. However, the meniscus is a large topographical barrier for millimeter-scale water-walking insects to pass from water surface to land. Because they are unable to use the traditional way to leap onto land, *Mesovelia* and infant water striders deform their body posture to surmount the menisci according to their intention. The wetting tips of the front and rear tarsi pull up the water surface, and the middle tarsi push down the water surface without breaking the free surface. With this fixed posture, the capillary forces are generated to propel them to ascend the menisci (*35*). On the basis of the same mechanism, the stimulus-responsive hydrogel water striders could climb the menisci on demand (Fig. 5, fig. S16, and movie S9). In the beginning, the flower-shaped hydrogel water strider moved in a combination of linear and circular motion in 2 s, as the gradient color illustrated trajectories showed. According to need, humidity stimulus was applied to the hydrogel water striders, and the eight petals of flower-shaped hydrogel water striders curved up. Then, the hydrogel water strider climbed the menisci and attached onto the interface of wall and water. As shown above, the hydrogel water striders at the water-air interface showed hydrophobic properties and moved away from the hydrophilic boundaries and land. However, the underwater part of the hydrogel was wetted and demonstrated hydrophilic features when encountering a hydrophilic boundary. Thus, the curved-up hydrogel water striders exposed the wetted surface at and above the water-air interface, which were attracted to and moved toward the hydrophilic land. In addition, the curved-up hydrogel water striders pulled up the free water surface and generated capillary force to ascend the menisci. On the basis of these two forces, the hydrogel water striders could quickly climb the menisci and attach to the target position as shown in the top view and side view photos in Fig. 5. Thus, the hydrogel water striders could move on the water surface freely with controllable motion and climb the menisci as required, which imitated all the locomotion of common water striders.

## DISCUSSION

We created hydrogels that can autonomously move on the surface of water (and potentially other liquids) with high speed and long

locomotion duration. We achieved locomotion through a dynamic wetting process without the need for external energy sources. Compared with conventional hydrogels as actuators, the autonomous locomotion of active hydrogel does not involve deformations or external stimuli. The locomotion of our active hydrogel is determined by the materials or geometry design of the hydrogel and its surrounding environment. Our hydrogel could potentially be used in environmental applications or for exploration. Another potential application involves adaptive aquatic missions, such as transporting cargo through complex environment to desired locations.

## MATERIALS AND METHODS

### Materials

Hydroxyethyl methacrylate and rhodamine B were supplied by Sigma-Aldrich. Ethylene glycol dimethyl acrylate (EGDMA), 2-hydroxy-2-methylpropiophenone, acrylic acid, methacrylic anhydride, NIPAM, azobenzene, AMPS, polyvinylpyrrolidone [molecular weight (Mw) = 1,300,000], $CoCl_2$, methyl violet, methyl orange, and erioglaucine disodium salt were obtained from Aladdin Company. PDMS (SYLGARD 184) was supplied by Dow Corning. All chemicals were used without further purification.

### Preparation of hydrogel precursor solution

Hydroxyethyl methacrylate (51.06 volume %), acrylic acid (21.28 volume %), and EGDMA (1.06 volume %) were mixed in a beaker and bubbled by nitrogen gas for 5 min. The photoinitiator 2-hydroxy-2-methylpropiophenone (26.60 volume %) was added into the mixture just before synthesis. Rhodamine B was also added for better visualization on water surface. During usage, the container of hydrogel precursor solution was protected from ultraviolet (UV) light by aluminum foil.

### Soft mold casting of the hydrogel

The hydrogel precursor solution was dropped into the PDMS mold and exposed to dual-wavelength UV light (254 and 365 nm) until the hydrogel was completely solidified. The lighting power density of the UV light was 0.21 W/cm$^2$. The pristine hydrogel was washed by deionized (DI) water to remove the uncross-linked residues and then stored in the dry cabinet.

### 3D printing of the hydrogel

We added 6.5 weight % polyvinylpyrrolidone into the hydrogel precursor solution to increase the viscosity and used a magnetic stirrer to stir the mixture for 10 hours at 700 rpm. We put the mixture into the syringe and loaded it into the 3D printing Work Station (Regenovo 3D Bio-Architect) with various nozzle sizes (from 0.16 to 0.60 mm in diameter). Printing paths were generated by computer-aided design drawings and converted into G-code. The extrusion pressure ranged from 0.05 to 0.45 MPa, and the printing speed ranged from 6 to 20 mm/s. During the printing process, UV light with a wavelength of 365 nm and power intensity of 0.21 W/cm$^2$ was shined on the nozzle to solidify the hydrogel.

### Preparation of stimuli-responsive hydrogel

#### *Temperature responsive*

NIPAM was dissolved in water to form an aqueous solution (0.2 g/ml). Then, the NIPAM aqueous solution (34.73 volume %) was mixed with hydroxyethyl methacrylate (33.33 volume %), acrylic acid (13.89 volume %), and EGDMA (0.69 volume %) and bubbled with nitrogen gas for 5 min. The photoinitiator 2-hydroxy-2-methylpropiophenone (17.36 volume %) was added to the mixture just before synthesis.

#### *Electrical responsive*

AMPS was dissolved in water to form an aqueous solution (0.1 g/ml). Then, the AMPS aqueous solution (9.62 volume %) was mixed with hydroxyethyl methacrylate (46.15 volume %), acrylic acid (19.23 volume %), and EGDMA (0.96 volume %) and bubbled with nitrogen gas for 5 min. The photoinitiator 2-hydroxy-2-methylpropiophenone (24.04 volume %) was added to the mixture just before synthesis.

#### *Optical responsive*

Azobenzene was dissolved into acrylic acid to form a solution (0.02 g/ml). Then, this solution (19.42 volume %) was mixed with hydroxyethyl methacrylate (46.60 volume %) and EGDMA (9.71 volume %) and bubbled with nitrogen gas for 5 min. The photoinitiator 2-hydroxy-2-methylpropiophenone (24.27 volume %) was added to the mixture just before synthesis.

### Hydrogel motion observation

All videos were recorded on a digital camera (SONY HDR-CX350E) mounted on a stabilizer. The container for hydrogel motion was a rectangular hydrophilic plastic container with a length of 0.9 m, a width of 0.4 m, and a depth of 0.3 m. All the water used in this study was DI water, and 5 liters of DI water was added to the container for the hydrogel locomotion each time.

### Characterizations of hydrogels

#### *Fourier transform infrared spectrum*

P(HEMA-co-AA) hydrogel with different cross-linker amounts ranging from 0.5 to 10 volume % and pHEMA, pMA, and algae-calcium hydrogels were fabricated into small round pieces with a diameter of 5 mm and a thickness of 1 mm. The Fourier transform infrared (FT-IR) absorbance spectrum ranged from 400 to 4000 cm$^{-1}$ by a FT-IR spectrometer (Nicolet 6700, Thermo Fisher Scientific).

#### *Contact angle measurement*

P(HEMA-co-AA) hydrogel was fabricated into a small round piece with a diameter of 1 cm and a thickness of 3 mm. Then, 3 μl of DI water was dropped onto the hydrogel surface every 5 min, and the contact angles were measured by the drop shape analyzer (DSA 30, Kruss) every 12 s.

#### *Rheological test*

The pristine hydrogel round pieces were hard and fragile, which made them infeasible to be fixed by the rheometer (Haake Mars III, Thermo Fisher Scientific). Thus, we measured the rheological properties of hydrogel after they moved on the water surface for 210 min. The elastic and viscosity modulus at a fixed shear strain of 0.5% were measured with scanning oscillation frequency, and those at a fixed oscillation frequency of 1.59 Hz were measured with scanning shear strain.

### In situ AFM

The pristine hydrogel was placed onto the sample stage of the AFM, and then, quantities of water were added onto the hydrogel surface. Then, an in situ fast-scan AFM (FastScan, Bruker) of hydrogel was conducted to get the microscopic modulus and morphologies during the water intake process.

#### *Cryo-SEM*

We conducted cryo-SEM to observe the morphology changes during the wetting process. The hydrogel samples were rapidly frozen in

liquid nitrogen and then cut with an installed cold knife and sputtered with Pt in cryogenic apparatuses. The sputtered specimens were observed by using the cryo-SEM in a cryogenic state, which was operated at a temperature of 193.15 K and an accelerating voltage of 5 kV.

## SUPPLEMENTARY MATERIALS

robotics.sciencemag.org/cgi/content/full/6/53/eabe7925/DC1
Fig. S1. FT-IR spectrum of different active hydrogels.
Fig. S2. Instantaneous velocity of hydrogel and the frequency of velocity changes.
Fig. S3. Using $CoCl_2$ as color indicator to visualize the velocity of hydrogel water striders.
Fig. S4. Modulus and morphology characterization of hydrogel during water intake process.
Fig. S5. Velocity and mass swelling ratio of one hydrogel water strider in nine repeating cycles.
Fig. S6. Velocity and mass swelling ratio of hydrogel with different amounts of cross-linkers ranging from 0.5 to 10 volume % and different types.
Fig. S7. AFM images of the hydrogel with different cross-linker amounts ranging from 0.5 to 10 volume %.
Fig. S8. Contact angle changes of hydrogels with different cross-linker amounts in 30 min.
Fig. S9. The velocity of p(HEMA-co-AA) hydrogel moving on different solutions with different surface tension coefficients.
Fig. S10. Locomotion of hydrogel water strider on aqueous solutions with different pH values.
Fig. S11. Photos of hydrogel processed by different methods.
Fig. S12. Locomotion of hydrogels with symmetric shapes.
Fig. S13. Energy of two menisci on infinitely long surfaces as a function of the separation between two surfaces with different wettability.
Fig. S14. Floating plastic debris collection and surface wettability identification via the hydrogel water strider.
Fig. S15. Controlled locomotion of hydrogel water strider through heat.
Fig. S16. Freewill locomotion and meniscus climbing of humidity- and pH-responsive hydrogel water strider.
Movie S1. Hydrogel water strider with asymmetric materials.
Movie S2. Hydrogel water strider with geometry asymmetry and different edge lengths.
Movie S3. Gear-shaped hydrogel water strider.
Movie S4. Hydrogel water strider in confined environment.
Movie S5. Hydrogel water strider in confined environment with opening.
Movie S6. Ball game–like locomotion.
Movie S7. Intelligent manipulation of objects.
Movie S8. Locomotion of different types of stimulus-responsive hydrogel water striders.
Movie S9. Freewill moving and meniscus climbing.
Movie S10. Plastic debris collection and surface wettability identification.

## REFERENCES AND NOTES


1. J. W. Glasheen, T. A. McMahon, A hydrodynamic model of locomotion in the basilisk lizard. *Nature* **380**, 340–342 (1996).
2. S. Lee, J. W. M. Bush, A. E. Hosoi, E. Lauga, Crawling beneath the free surface: Water snail locomotion. *Phys. Fluids* **20**, 082106 (2008).
3. J. W. M. Bush, D. L. Hu, M. Prakash, The integument of water-walking arthropods: Form and function. *Adv. Insect Physiol.* **34**, 117–192 (2007).
4. D. L. Hu, B. Chan, J. W. M. Bush, The hydrodynamics of water strider locomotion. *Nature* **424**, 663–666 (2003).
5. X. Gao, L. Jiang, Water-repellent legs of water striders. *Nature* **432**, 36–36 (2004).
6. D. L. Hu, J. W. M. Bush, The hydrodynamics of water-walking arthropods. *J. Fluid Mech.* **644**, 5–33 (2010).
7. J. Song, F. Guan, W. Pan, Z. Liu, J. Sun, S. Ling, X. Deng, Y. Sun, Droplet-based self-propelled miniboat. *Adv. Funct. Mater.* **30**, 1910778 (2020).
8. M. Kaynak, A. Ozcelik, N. Nama, A. Nourhani, P. E. Lammert, V. H. Crespi, T. J. Huang, Acoustofluidic actuation of in situ fabricated microrotors. *Lab Chip* **16**, 3532–3537 (2016).
9. A. A. Solovev, Y. Mei, O. G. Schmidt, Catalytic microstrider at the air-liquid interface. *Adv. Mater.* **22**, 4340–4344 (2010).
10. S. K. Sailapu, A. Chattopadhyay, Induction of electromotive force by an autonomously moving magnetic bot. *Angew. Chemie.* **126**, 1547–1550 (2014).
11. X. Liu, J. Liu, S. Lin, X. Zhao, Hydrogel machines. *Mater. Today* **36**, 102–124 (2020).
12. O. Erol, A. Pantula, W. Liu, D. H. Gracias, Transformer hydrogels: A review. *Adv. Mater. Technol.* **4**, 1900043 (2019).
13. H. Yuk, S. Lin, C. Ma, M. Takaffoli, N. X. Fang, X. Zhao, Hydraulic hydrogel actuators and robots optically and sonically camouflaged in water. *Nat. Commun.* **8**, 14230 (2017).
14. Y. Dong, J. Wang, X. Guo, S. Yang, M. O. Ozen, P. Chen, X. Liu, W. Du, F. Xiao, U. Demirci, B.-F. Liu, Multi-stimuli-responsive programmable biomimetic actuator. *Nat. Commun.* **10**, 4087 (2019).
15. Y. Zhao, C. Xuan, X. Qian, Y. Alsaid, M. Hua, L. Jin, X. He, Soft phototactic swimmer based on self-sustained hydrogel oscillator. *Sci. Robot.* **4**, eaax7112 (2019).
16. H. Wang, Y. Liang, W. Gao, R. Dong, C. Wang, Emulsion hydrogel soft motor actuated by thermal stimulation. *ACS Appl. Mater. Interfaces* **9**, 43211–43219 (2017).
17. W. Zhu, J. Li, Y. J. Leong, I. Rozen, X. Qu, R. Dong, Z. Wu, W. Gao, P. H. Chung, J. Wang, S. Chen, 3D-printed artificial microfish. *Adv. Mater.* **27**, 4411–4417 (2015).
18. F. J. Holly, M. F. Refojo, Wettability of hydrogels I. Poly(2-hydroxyethyl methacrylate). *J. Biomed. Mater. Res.* **9**, 315–326 (1975).
19. Q. Chen, D. Zhang, G. Somorjai, C. R. Bertozzi, Probing the surface structural rearrangement of hydrogels by sum-frequency generation spectroscopy. *J. Am. Chem. Soc.* **121**, 446–447 (1999).
20. H. Yasuda, A. K. Sharma, T. Yasuda, Effect of orientation and mobility of polymer molecules at surfaces on contact angle and its hysteresis. *J. Polym. Sci. Polym. Phys. Ed.* **19**, 1285–1291 (1981).
21. J. D. Andrade, D. E. Gregonis, L. M. Smith, Polymer surface dynamics, in *Surface and Interfacial Aspects of Biomedical Polymers* (Springer, 1985), pp. 15–41.
22. K. B. Lewis, B. D. Ratner, Observation of surface rearrangement of polymers using ESCA. *J. Colloid Interface Sci.* **159**, 77–85 (1993).
23. K. Kato, E. Uchida, E.-T. Kang, Y. Uyama, Y. Ikada, Polymer surface with graft chains. *Prog. Polym. Sci.* **28**, 209–259 (2003).
24. L. E. Scriven, C. V. Sternling, The marangoni effects. *Nature* **187**, 186–188 (1960).
25. N. A. Peppas, H. J. Moynihan, L. M. Lucht, The structure of highly crosslinked poly(2-hydroxyethyl methacrylate) hydrogels. *J. Biomed. Mater. Res.* **19**, 397–411 (1985).
26. P. J. Flory, *Principles of Polymer Chemistry* (Cornell Univ. Press, 1953).
27. W. Wang, Y.-Q. Liu, Y. Liu, B. Han, H. Wang, D.-D. Han, J.-N. Wang, Y.-L. Zhang, H.-B. Sun, Direct laser writing of superhydrophobic PDMS elastomers for controllable manipulation via Marangoni Effect. *Adv. Funct. Mater.* **27**, 1702946 (2017).
28. N. Bowden, A. Terfort, J. Carbeck, G. M. Whitesides, Self-assembly of mesoscale objects into ordered two-dimensional arrays. *Science* **276**, 233–235 (1997).
29. B. A. Grzybowski, N. Bowden, F. Arias, H. Yang, G. M. Whitesides, Modeling of menisci and capillary forces from the millimeter to the micrometer size range. *J. Phys. Chem. B* **105**, 404–412 (2001).
30. J. Simmchen, J. Katuri, W. E. Uspal, M. N. Popescu, M. Tasinkevych, S. Sánchez, Topographical pathways guide chemical microswimmers. *Nat. Commun.* **7**, 10598 (2016).
31. S. E. Spagnolie, E. Lauga, Hydrodynamics of self-propulsion near a boundary: Predictions and accuracy of far-field approximations. *J. Fluid Mech.* **700**, 105–147 (2012).
32. W. E. Uspal, M. N. Popescu, S. Dietrich, M. Tasinkevych, Rheotaxis of spherical active particles near a planar wall. *Soft Matter* **11**, 6613–6632 (2015).
33. Z. Xiao, M. Wei, W. Wang, A review of micromotors in confinements: Pores, channels, grooves, steps, interfaces, chains, and swimming in the bulk. *ACS Appl. Mater. Interfaces* **11**, 6667–6684 (2019).
34. E. M. Purcell, Life at low Reynolds number. *Am. J. Phys.* **45**, 3–11 (1977).
35. D. L. Hu, J. W. M. Bush, Meniscus-climbing insects. *Nature* **437**, 733–736 (2005).


**Acknowledgments:** We thank S. Li and C. Liu for the water strider collection and Z. Tian for helpful discussions. **Funding:** This work was supported by the National Natural Science Foundation of China (nos. 51961145108, 61975035, and 51603044) and the Program of Shanghai Academic Research Leader (no. 19XD1400600). **Author contributions:** Y.M., B.X., and H.Z. designed the experiments. H.Z. performed all experiments. X.P. performed the 3D printing of designed materials. Z.Q. conducted AFM characterization of the hydrogel. H.Z. and YM. analyzed all data, and B.X., Y.W., and Z.Q. analyzed part of the data. H.Z. and Y.M. prepared the manuscript. All authors read, contributed, and approved the final manuscript. **Competing interests:** Y.M. and H.Z. are inventors on a patent application (no. CN202011346652.2) submitted by Fudan University that covers the fabrication methods of the smart hydrogels. The other authors declare that they have no competing interests. **Data and materials availability:** All data are available in the main text or the Supplementary Materials.

Submitted 15 September 2020
Accepted 22 March 2021
Published 14 April 2021
10.1126/scirobotics.abe7925

**Citation:** H. Zhu, B. Xu, Y. Wang, X. Pan, Z. Qu, Y. Mei, Self-powered locomotion of a hydrogel water strider. *Sci. Robot.* **6**, eabe7925 (2021).

Science Robotics

# Self-powered locomotion of a hydrogel water strider

Hong Zhu, Borui Xu, Yang Wang, Xiaoxia Pan, Zehua Qu, and Yongfeng Mei

*Sci. Robot.* **6** (53), eabe7925. DOI: 10.1126/scirobotics.abe7925







*Science Robotics* (ISSN 2470-9476) is published by the American Association for the Advancement of Science. 1200 New York Avenue NW, Washington, DC 20005. The title *Science Robotics* is a registered trademark of AAAS.